Latency and Reliability of mmWave Multi-Hop V2V Communications Under Relay Selections

Zipeng Li, *Student Member, IEEE*, Lin Xiang, *Member, IEEE*, Xiaohu Ge, *Senior Member, IEEE*, Guoqiang Mao, *Fellow, IEEE*, and Han-Chieh Chao, *Senior Member, IEEE*

***Abstract*—Timely and reliable information sharing among autonomous vehicles (AVs) provides a promising approach for reducing traffic congestion and improving traffic efficiency in future intelligent transportation systems. In this paper, we consider millimeter-wave (mmWave) based multi-hop vehicle-to-vehicle (V2V) communications to facilitate ultra-reliable low-latency information sharing among AVs. We propose a novel framework for performance analysis and design of relay selection schemes in mmWave multi-hop V2V communications, while taking into account the mmWave signal propagation characteristics, road topology, and traffic conditions. In particular, considering the minimum tracking distance requirement of road traffic, the headway, i.e., the distance between adjacent AVs, is modeled as shifted-exponential distribution. Moreover, we model the communication path losses using the Manhattan distance metric in the taxicab geometry, which can more accurately capture the characteristics of mmWave signal propagation in urban grid roads than conventional Euclidean distance geometry. Based on the proposed model, we investigate the latency and reliability of mmWave multi-hop V2V communications for three widely adopted relay selection schemes, i.e., random with forward progress (RFP), most forward with fixed radius (MFR), and nearest with forward progress (NFP), respectively. Furthermore, we propose a novel relay selection scheme for joint optimization of the single-hop forward progress (FP) and single-hop latency according to the AVs' instantaneous locations and an estimate of the residual multi-hop latency. Simulation results show that, by balancing the current single-hop latency and the residual multi-hop latency for the multi-hop V2V network, the proposed relay selection scheme significantly outperforms the MFR, NFP and RFP in both multi-hop transmission latency and reliability of mmWave V2V communications.**

***Index Terms*—Latency, reliability, autonomous vehicles (AVs), multi-hop vehicle-to-vehicle (V2V) communications, millimeter-wave (mmWave), relay selections.**

Manuscript received June 24, 2019; revised November 23, 2019 and April 12, 2020; accepted June 4, 2020. Date of publication June 16, 2020; date of current version October 13, 2020. This work was supported by the National Key Research and Development Program of China under Grant 2017YFE0121600. The review of this article was coordinated by Prof. S. Coleri. *(Corresponding author: Xiaohu Ge.)*

Zipeng Li and Xiaohu Ge are with the School of Electronic Information and Communications, Huazhong University of Science and Technology, Wuhan 430074, China (e-mail: zipengli91@hust.edu.cn; xhge@mail.hust.edu.cn).

Lin Xiang is with Institute for Digital Communications (IDC), Friedrich-Alexander University of Erlangen-Nuremberg (FAU), D-91058 Erlangen, Germany (e-mail: lin.xiang@fau.de).

Guoqiang Mao is with the School of Computing and Communications, University of Technology Sydney, Sydney, NSW 2007, Australia (e-mail: guoqiang.mao@uts.edu.au).

Han-Chieh Chao is with the Department of Electrical Engineering, National Dong Hwa University, Hualien 97401, Taiwan (e-mail: hcc@ndhu.edu.tw).

Digital Object Identifier 10.1109/TVT.2020.3002903

I. Introduction

MILLIMETER-WAVE (mmWave) is a key technology to meet the communication demands of autonomous vehicles (AVs) in the fifth-generation (5G) mobile communication systems and beyond [1], [2]. In particular, the large bandwidth of mmWave signals can be exploited to facilitate ultra-reliable low-latency vehicle-to-vehicle (V2V) communications. This provides a promising approach for sharing environment information among AVs to reduce traffic congestion and to improve the efficiency of future intelligent transportation systems. However, the mmWave signals have only a limited transmission range, which may hinder direct communications among the AVs, especially if the AVs are located far apart. Therefore, multi-hop V2V communication in the mmWave spectrum is usually preferred for AVs as it can enhance mmWave signal propagation with minimum or without aid of mobile communication infrastructures [3], [4]. In this case, intelligent selection of the relaying AVs is crucial to facilitate timely and reliable V2V message transmission.

The performance of mmWave multi-hop V2V communication in urban scenarios depends critically on the mmWave signal propagation characteristics, road topology, time-varying traffic loads, as well as the spatial distributions of vehicles, which can be intricate to analyze. For example, due to excess blockages from buildings and pedestrians on both sides of urban roads, the energy of mmWave signals would propagate mainly along the roads. Consequently, the propagation paths of mmWave signals will depend critically on the topology of the urban roads, which does not fit the conventional Euclidean geometry.[1] Moreover, the communication distances between source and relay/destination AVs as well as the locations of potential interfering AVs may vary significantly over time due to the moving AVs, the unpredictable traffic loads, and the adopted relay selection criteria. As a result, communication latency and reliability may fluctuate intermittently. To tackle these challenges, a unified framework for modeling and analyzing the latency and reliability of mmWave multi-hop V2V communications is needed, particularly in real-life urban scenarios.

Several works have analyzed the performance of multi-hop V2V communications in the sub-6 GHz cellular spectrum [5]–[8]. In [5], S. Li *et al.* proposed a novel link quality indicator

[1]For example, AVs are located and transported only within confined areas or strips according to the road layout rather than in the whole Euclidean plane. In this case, the Euclidean distance would be inadequate for modeling the tracking distance between the AVs.

to evaluate the latency and reliability of message transmission over interference-free wireless V2V links. The results in [5] revealed that, for given vehicle density, there exists an optimal communication distance in each hop that maximizes the performance of the source-to-destination link. Considering a multi-lane highway scenario in [6], multi-hop V2V communications employing carrier-sense multiple access (CSMA) were investigated for several packet forwarding schemes, where an interesting trade-off between the single-hop forward progress (FP), i.e., the distance that a packet has traveled towards its final destination, and the success probability of message transmission was unveiled. In [7], the authors investigated the performance of message broadcast over multi-hop V2V links, where the impact of single-hop link distance and vehicle density on the communication latency was evaluated. By modeling the vehicle locations on orthogonal streets as a Poisson point process (PPP), Jeyaraj *et al.* investigated interfering V2V transmissions in urban cities and derived the closed-form expression for the successful transmission probability between adjacent vehicles [8]. The results in [8] revealed that the performance of the considered V2V communications is severely limited in the presence of interfering vehicles on the same street.

On the other hand, the application of mmWave for improving the performance of V2V communications has recently been investigated in [9]–[12]. In [9], by modeling the streets using a line process, Ozpolat *et al.* analyzed the network coverage for urban mmWave vehicular ad hoc networks. It was shown in [9] that mmWave links can enable reliable V2V communications even in the heavy traffic scenario. Based on the stochastic geometry theory, the line-of-sight (LoS) and non-LoS interference caused by vehicles on the side lanes were evaluated for mmWave V2V communications in highways and urban road environments [10]. The results in [10] showed that the interference power strongly depends on the directivity of mmWave antennas. In [11], distributed vehicle association and beam alignment for mmWave V2V networks were investigated using matching theory and swarm intelligence. The authors of [11] further proposed a cross-layer link scheduling scheme for minimizing the transmission latency of mmWave V2V networks. In [12], Wu *et al.* proposed a novel information-centric networking (ICN) protocol and a decentralized vehicle association algorithm to achieve low-latency content dissemination in mmWave vehicular networks. By enabling vehicles to cache contents at the network edge, the authors in [12] showed that the content retrieval latency can be significantly reduced.

To further improve the performance of multi-hop V2V communications, several relay selection schemes have been proposed in the literature [13]–[16]. In [13], Feteiha *et al.* proposed a novel multi-hop transmission scheme for V2V communication in a highway scenario, where the relaying vehicle that maximizes the receiving signal-to-noise ratio (SNR) is selected per transmission hop. Considering multi-hop MIMO transmissions, relay selection for maximization of the receiving SNR was investigated for a two-lane vehicular network in [14]. Simulation results in [14] showed that the proposed relay selection scheme achieves large performance gains at the expense of increased computational complexity. In [15], two relay vehicle selection schemes were proposed for V2V communication in a dense multi-lane highway scenario. The authors of [15] analysed the outage probability and the throughput of the proposed schemes assuming Nakagami-m fading channels. In [16], Sun *et al.* proposed a routing scheme for vehicular ad hoc networks, which can exploit parked vehicles to improve link quality and reduce packet delivery latency.

The aforementioned works [5]–[9] have modeled the locations of AVs along the roads as a one-dimensional (1D) PPP. Thereby, the headway, i.e., the distance between adjacent AVs, follows an exponential distribution, which allows the AVs to drive close to each other with a non-negligible probability. In real-life scenarios, however, a minimum tracking distance between adjacent AVs is mandatory for ensuring driving safety but fails to be captured by the 1D PPP model. Moreover, the aforementioned works [9]–[16] have modeled the signal propagation distances using the Euclidean distance between AVs. This can be quite inaccurate for analyzing urban scenarios, where the mmWave signals may not penetrate the buildings located alongside the roads but mainly propagate along the urban roads. In this case, the propagation distance of mmWave signals is more accurately estimated by the total length of the urban roads that they have traversed than the Euclidean distance [17]. Due to these limitations, the existing models may lead to inaccurate performance analyses and inefficient relay selection designs for mmWave multi-hop V2V communications in urban scenarios.

To bridge the knowledge gaps, in this paper, we consider a novel framework of stochastic geometry for modeling mmWave multi-hop V2V communications in urban roads and for designing the relay selection scheme. We note that the stochastic geometry framework has been shown as a tractable and promising tool for modeling and performance analysis of large-scale cellular networks [18] and V2V networks [19]; therefore, it is adopted in this paper. In particular, we model the headway using shifted-exponential distribution (SED), which is an exponential distribution with its support shifted by a constant. The SED based headway model not only captures the characteristic of free traffic flows on urban roads, but also ensures a minimum tracking distance between adjacent AVs on the same road subject to driving safety requirement. Moreover, considering urban roads of typical grid topology, the propagation distance of mmWave signals is modeled using the Manhattan distance between AVs. Thereby, the performance analysis has to be newly considered in the taxicab geometry, which differs significantly from the conventional Euclidean distance based analysis. However, due to statistical modeling of the AVs' locations, the network performance obtained using stochastic geometry may not facilitate accurate decisions for an individual AV. To tackle this issue, we further propose a relay selection scheme for each AV, which aims to minimize the multi-hop latency according to the instantaneous locations of AVs sensed within the transmission range of each host AV and the potential latency of residual hops. To facilitate convenient performance analysis and optimization in the considered taxicab geometry, we only investigate interference-free mmWave multi-hop V2V communications throughout this paper. Nevertheless, the adoption of interference-free versus

TABLE I
LIST OF KEY NOTATIONS

Symbol	Description	Symbol	Description
V_t, V_r, V_d	Source, relay and destination AVs	d_x, d_y	Intervals of adjacent horizontal and vertical roads
D_{adj}	Headway	d_s	Minimum tracking distance between adjacent AVs on the same road
μ	Average road traffic load	d_0	Distance between V_t and V_d
P_{tx}	Transmit power of AVs	d_t	Effective communication range of AVs
$l_{i,j}$	Single-hop link between transmitter V_i and receiver V_j	$g_{i,j}^{\text{tx}}$, $g_{i,j}^{\text{rx}}$	Transmitter and receiver directivity gains in link $l_{i,j}$
$G_{\measuredangle}$, $g_{\measuredangle}$	Main-lobe and side-lobe antenna gains	$\beta_{i,j}^{\varphi}$	Alignment error for AVs V_i and V_j
$G_{i,j}^{\text{c}}$	Channel gain of link $l_{i,j}$	ρ	Shadowing
σ	Standard deviation of shadowing	α	Path loss exponent
$D_{M,i,j}$	Manhattan distance between V_i and V_j	t_t	Duration of packet transmission
τ	Beam alignment latency	$\psi_{i,j}^{\text{tx}}$, $\psi_{i,j}^{\text{rx}}$	Sector-level beamwidths of V_i and V_j per iteration
$\varphi_{i,j}^{\text{tx}}$, $\varphi_{i,j}^{\text{rx}}$	Beam-level beamwidths of V_i and V_j per iteration	t_p	Duration of pilot transmission
$R_{i,j}$	Effective data rate achievable on link $l_{i,j}$	$\text{SNR}_{i,j}$	SNR of link $l_{i,j}$
N_0	Noise power spectral density	B	Bandwidth of mmWave signals
P_S	Packet size	T_{one}	Transmission latency for a typical single-hop link
T_{mul}	Multi-hop latency	$\mathbb{E}(K)$	Average hop count
t_{pro}	Signal processing the latency at relay AV	Z	FP of a typical single-hop link
P_{one}	Transmission reliability of a typical single-hop link	ε	SNR threshold
P_{mul}	Multi-hop reliability	$d(\text{E})$, $S(\text{E})$	Road length and area of region E
Φ_i	Set of AVs within the effective communication range of V_i and having positive FP	$\Phi_i{}'$	Subset of Φ_i with $\mathbb{E}(\text{SNR}) \geqslant \varepsilon_0$

interfering V2V communications is still much debated and one may refer to [5], [6], [8], [10], for more intriguing discussions.

The contributions of this paper are summarized as follows:

1) We propose a novel framework of stochastic taxicab geometry for modeling interference-free mmWave multi-hop V2V communication networks, where the headway is modeled as SED to ensure the minimum tracking distance between adjacent AVs. Moreover, the propagation distance of mmWave signal between AVs is characterized using the Manhattan distance between AVs.
2) Based on the proposed framework, we analyze the latency and reliability of message transmission in the considered mmWave multi-hop V2V networks for three commonly adopted forwarding schemes, i.e., random with forward progress (RFP), most forward with fixed radius (MFR) and nearest with forward progress (NFP), which select a random AV, the AV with the largest FP, and the AV with the smallest FP within the effective communication range for message forwarding, respectively. Analytical expressions for characterizing the performance of mmWave multi-hop V2V communications are provided.
3) We further propose a novel relay selection scheme based on the joint optimization of single-hop FP and single-hop latency. Simulation results show that the proposed relay scheme outperforms the RFP, MFR and NFP schemes in both multi-hop transmission latency and reliability of the message.

The remainder of this paper is organized as follows. The system model of mmWave multi-hop V2V communications in urban scenarios is presented in Section II. In Section III, based on the SED headway, we analyze the latency and reliability of message transmission over multi-hop V2V links for RFP, MFR and NFP schemes, respectively. By joint optimization of single-hop FP and latency, the proposed relay selection scheme is introduced in Section IV. Section V presents the simulation results and, finally, Section VI concludes the paper. The key notations used in this paper are summarized in Table I.

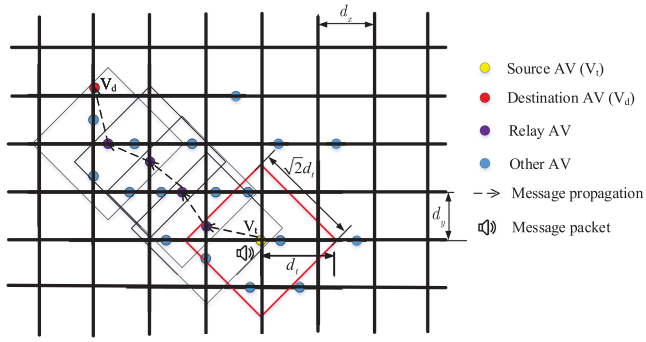

Fig. 1. Network model for mmWave multi-hop V2V communications on urban roads of grid topology.

II. SYSTEM MODEL

In this section, we present the system model for mmWave multi-hop V2V communications on urban roads.

A. Network Model

We consider an mmWave V2V communication network in the urban scenario as shown in Fig. 1 [20]. The urban roads have a typical grid topology as in e.g. metropolitan cities, where the horizontal and the vertical roads intersect into line segments of lengths d_x and d_y, respectively. We assume that the widths of the roads are negligible compared to d_x and d_y, for which they have

negligible impact on the performance of V2V communications[2] and, hence, are ignored in the system model.

For purpose of performance analysis, we assume at the moment that the AVs on the urban roads are spatially randomly distributed. However, this assumption will be removed in Section IV when we consider the design of the relay selection algorithm. As adjacent moving AVs have to respect a minimum tracking distance to avoid traffic accidents caused by e.g. crash and rear-end collision, 1D PPP is inaccurate for modeling the positions of AVs in the considered network. In the following, we propose an SED headway model to characterize the spatial distributions of AVs. Thereby, the headway comprises two components, i.e., $D_{\rm adj} = d_s + W$ [21], where d_s is a constant and denotes the minimum tracking distance between adjacent AVs on the same road subject to driving safety requirement. W is a random variable and follows an exponential distribution with mean $\frac{1}{\mu}$. Consequently, the cumulative distribution function (CDF) of $D_{\rm adj}$ is given by

$$F_{D_{\rm adj}}\left(d_{\rm adj}\right) = \begin{cases} 0, & \text{for } d_{\rm adj} < d_s, \\ 1 - e^{-\mu\left(d_{\rm adj} - d_s\right)}, & \text{for } d_{\rm adj} \geqslant d_s. \end{cases} \quad (1)$$

The mean value of $D_{\rm adj}$ is given as $\mathbb{E}(D_{\rm adj}) = 1/\lambda$, where $\lambda = \mu/(1 + \mu d_s)$ captures the average road traffic load in the considered vehicular network after taking μ and d_s into account. We note that the proposed SED headway model is more general than the 1D PPP and reduces to the latter when $d_s = 0$.

As shown in Fig. 1, a typical AV located at the crossroad, denoted as V_t, needs to send a message about e.g. traffic information, road condition, etc., to AV V_d, which is located at an Euclidean distance of d_0 away from V_t, while V_t keeps driving through the crossroad. The AVs are equipped with mmWave transceivers and employ transmit power $P_{\rm tx}$. Due to excess blockages on both sides of the urban roads, the mmWave signals are assumed to propagate only along the grid roads. Moreover, the effective communication range of the AVs is limited to be within d_t, where $d_t < d_0$ as mmWave signals are prone to attenuation. Taking into account the grid topology of the considered urban roads, the effective communication range of each AV is given by the square centered at the AV, which has sides of length $\sqrt{2}d_t$ and is oriented at 45° to each coordinate axis as shown in Fig. 1. As each point on this square has a Manhattan distance of d_t to the center, it is also referred to as a taxicab circle of radius d_t in the taxicab geometry [22]. The AVs located within the effective communication range of V_t can initiate communications with V_t directly, whereas the other AVs have to communicate with V_t through the help of relays.

For a timely and reliable transmission of the message from V_t to V_d, the relay AVs are judiciously selected between V_t and V_d [23]. Moreover, after an AV is selected for message forwarding, only the transmission from the current AV to the selected relay AV is allowed within the effective communication range, i.e., the other AVs within the effective communication range of the selected relay AV remain silent. This can be achieved using e.g. carrier-sense multiple access with collision avoidance (CSMA/CA) [24, Ch. 14.3.3]. In particular, each AV senses the channel before accessing it and would back off from transmitting any packet over a busy channel. Once the channel becomes available, a potential transmitting AV requests for data packet transmission by sending a short request-to-send (RTS) packet. The potential receiver has to respond a clear-to-send (CTS) packet to acknowledge the start of data packet transmission that follows. To avoid collisions, the AVs overhearing the RTS or CTS packet, i.e., those locating within the communication range of the transmitting AV and the receiving AV, remain silent during the expected packet duration. As such, each AV would not be interfered by other AVs located within its communication range. Similar techniques have also been considered in [25]–[27] to mitigate interference. The selected relay AV decodes the received message and forwards it to the next-hop AV.[3] This process continues until the destined AV is finally reached. We note that, interference-free transmission is desirable particularly for avoiding strong LoS interference from AVs located on the same road as the transmitting AV [8]. However, it may come at a price of increased latency and overhead.[4]

B. Antenna Pattern and Channel Model

Each AV is equipped with an mmWave antenna array and employs directional beamforming to enhance mmWave signal propagation. For maximizing the directivity gains of mmWave antennas, the beam alignment is performed at both the transmitter and the receiver, as will be detailed in Section II-C. The generated directional antenna pattern after beam alignment is approximated by an ideal sector model in the horizontal plane [29]. In particular, denote the single-hop link between transmitter V_i and next-hop receiver V_j as $l_{i,j}$. The directivity gains $g_{i,j}^{\wp}$, $\wp \in \{\rm tx, rx\}$, of the transmitting and receiving AVs over link $l_{i,j}$ after beam alignment are given as

$$g_{i,j}^{\wp} = \begin{cases} G_{\lhd}, & \text{if } \left|\beta_{i,j}^{\wp}\right| \leqslant \varphi_{i,j}^{\wp}/2, \\ g_{\lhd}, & \text{otherwise}, \end{cases} \quad (2)$$

where $g_{i,j}^{\rm tx}$ and $g_{i,j}^{\rm rx}$ denote the transmission and reception directivity gains, respectively. $G_{\lhd}$ and $g_{\lhd}$ are the main-lobe and side-lobe antenna gains, respectively. Finally, $\beta_{i,j}^{\wp}$ models the tolerable alignment error in the antenna steering directions of transmitter V_i and receiver V_j, and $\varphi_{i,j}^{\wp}$ is the beamwidth.

To characterize the mmWave signal propagation in the considered network, we adopt the 72 GHz mmWave channel model as in [30]. Thereby, the channel gain in decibels, $g_{i,j}^{\rm c}[\rm dB](\bullet)$, of a typical single-hop link $l_{i,j}$ is given as

$$g_{i,j}^{\rm c}[\rm dB]\left(D_{M,i,j}\right) = -69.6 - 10\alpha \log_{10}\left(D_{M,i,j}\right) - \rho, \quad (3)$$

where $\rho \sim N(0, \sigma^2)$ models the shadowing attenuation in decibels with standard deviation σ. Moreover, α and $D_{M,i,j}$ are the

[2]Otherwise, the widths of the roads can be taken into account in d_x and d_y.

[3]In this article, we only consider decode-and-forward relaying [28], whereas the proposed modeling and performance analysis framework can be extended to other relaying schemes as well.

[4]It was evaluated in [26] that, by properly configuring the backoff time window, the latency incurred by CSMA/CA can be lowered to 56 μs. As this latency is negligible compared with the duration of data packet transmission, which usually takes several milliseconds, cf. Sec. V, its impact on the system performance is ignored in this article.

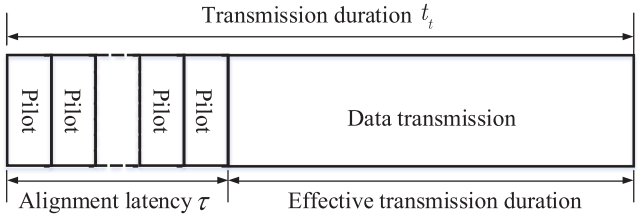

Fig. 2. Frame structure for beam alignment and data transmission in the considered mmWave V2V communication network.

path loss exponent and the propagation distance of mmWave signals between V_i and V_j, respectively. For mmWave V2V communications in grid urban roads, $D_{M,i,j}$ is more properly captured by the Manhattan distance between V_i and V_j than the Euclidean distance. In particular, given the Cartesian coordinates $V_i(x_i, y_i)$ and $V_j(x_j, y_j)$, we have $D_{M,i,j} = |x_i - x_j| + |y_i - y_j|$, i.e., the sum of lengths by projecting line segment V_iV_j onto the horizontal and vertical roads [31]. For the AVs with spatially random locations, $D_{M,i,j}$ is a random variable.

C. Latency and Reliability of mmWave Multi-Hop V2V Communications

Although multi-hop V2V communications can reduce the propagation loss of mmWave signals and enhance the reliability of message transmission between AVs V_t and V_d, it may penalize the overall transmission latency due to the increased number of communication hops [28]. Therefore, for the mmWave multi-hop V2V network, a comprehensive analysis of the latency and reliability taking into account the road and network topologies, mmWave signal propagation characteristics, and the adopted relay selection protocols is crucial, which will be discussed herein and in Section III.

1) Latency Analysis: Let P_S be the packet size of the message. Due to the large data rate enabled by mmWave V2V communications and the relatively small size of P_S, the latency incurred for completing a packet transmission is usually within tens of milliseconds, cf. Section V. Meanwhile, the speed of a mobile AV is typically in the range of 0∼40 km/h on urban roads [32]. This implies that, during each packet transmission, the changes in the AVs locations are only within decimeters[5] such that the path loss of the multi-hop links remains almost unchanged. Therefore, the impact of AV mobility on the performance of each packet transmission is negligible. For convenience of mathematical modeling, we assume that the positions of the AVs remain the same during a packet transmission.

We consider the frame structure as shown in Fig. 2, where the packet transmission of duration t_t comprises a beam alignment phase of duration τ and a data transmission phase of duration $t_t - \tau$. We adopt a two-stage beam alignment as proposed in [33]. In the first stage, sector-level alignment is achieved through a sequence of pilot transmissions, where the best sectors for the transmitter and the receiver are detected using an iterative trial-and-error approach. In the second stage, a fine-granularity beam-level sweep search is performed within the detected sectors to achieve beam-level alignment of the mmWave antennas.

In general, the latency incurred by the sector-level alignment is negligible compared with that by beam-level alignment [34]. Assuming that an exhausted iterative search has been adopted for beam-level alignment, the overall alignment latency in link $l_{i,j}$ is estimated as [34]

$$\tau = \frac{\psi_{i,j}^{\mathrm{tx}} \psi_{i,j}^{\mathrm{rx}}}{\varphi_{i,j}^{\mathrm{tx}} \varphi_{i,j}^{\mathrm{rx}}} t_p, \tag{4}$$

where $\psi_{i,j}^{\mathrm{tx}}$ and $\psi_{i,j}^{\mathrm{rx}}$ are the sector-level beamwidths of transmitter V_i and receiver V_j per iteration, respectively. $\varphi_{i,j}^{\mathrm{tx}}$ and $\varphi_{i,j}^{\mathrm{rx}}$ are the beam-level beamwidths of transmitter V_i and receiver V_j per iteration, respectively. t_p is the duration of one pilot transmission and $t_p \ll \tau$. Data transmission from transmitter V_i to receiver V_j is initiated after the beam alignment on link $l_{i,j}$ has been completed. During data transmission, the effective data rate achievable on the typical single-hop link $l_{i,j}$ is

$$R_{i,j} = \left(1 - \frac{\tau}{t_t}\right) B \log_2 \left(1 + \mathrm{SNR}_{i,j}\right), \tag{5}$$

where $\mathrm{SNR}_{i,j}$ is the SNR of link $l_{i,j}$,

$$\mathrm{SNR}_{i,j} = \frac{P_{\mathrm{tx}} g_{i,j}^{\mathrm{tx}} g_{i,j}^{c} g_{i,j}^{\mathrm{rx}}}{N_0 B}. \tag{6}$$

Herein, N_0 is the noise power spectral density and B is the bandwidth of the mmWave signal. In this paper, we consider perfect beam alignment, i.e., $|\beta_{i,j}^{\wp}| \leqslant \varphi_{i,j}^{\wp}/2$ holds. According to (2), the antenna gains of V_i and V_j are given by $G_{\triangleleft}$. Substituting (3) into (6), the SNR of $l_{i,j}$ in decibels is a random variable given as

$$\begin{aligned} &\mathrm{SNR}_{i,j}[\mathrm{dB}] \\ &= P_{\mathrm{tx}}[\mathrm{dBm}] - N_0[\mathrm{dBm/Hz}] - 10\log_{10}\left(B\,[\mathrm{Hz}]\right) \\ &\quad + 2G_{\triangleleft}[\mathrm{dB}] - 10\alpha \log_{10}\left(D_{M,i,j}\right) - 69.6 - \rho. \end{aligned} \tag{7}$$

The analysis of the typical single-hop link can be extended to other links in a straightforward manner [27], [35]. Hence, with a slight abuse of notations, the subscripts i and j in (2)–(7) will be dropped in the following analysis [36]. For example, $\mathrm{SNR}_{i,j}$ is rewritten as SNR. Then, the CDF of SNR in a single-hop link is derived as

$$\begin{aligned} F_{\mathrm{SNR}}(\gamma) &= \mathbb{P}\left\{\mathrm{SNR} \leqslant \gamma\right\} \\ &= \mathbb{P}\left\{u - 10\alpha \log_{10}\left(D_M\right) - \rho \leqslant \gamma\,[\mathrm{dB}]\right\} \\ &\overset{(a)}{=} \frac{1}{2} - \frac{1}{2}\mathbb{E}\left[W\left(\gamma, D_M\right)\right] \\ &= \frac{1}{2} - \frac{1}{2}\int_0^{+\infty} W\left(\gamma, d_M\right) f_{D_M}\left(d_M\right) dd_M, \end{aligned} \tag{8}$$

[5]For packet sizes given in Section V, our simulation results show that the multi-hop latency required for both 72 GHz mmWave band and 5.9 GHz band transmissions are usually within 30 milliseconds. This implies that, during a packet transmission, the AV moves by at most $40 \times 1000 \div 3600 \times 0.03 \approx 0.33$ m.

with

$$W\left(\gamma, D_M\right) = \mathrm{erf}\left[\frac{u - 10\log_{10}\gamma - 10\alpha\log_{10}\left(D_M\right)}{\sqrt{2}\sigma}\right], \quad (9)$$

where $u = P_{\mathrm{tx}}[\mathrm{dBm}] - N_0[\mathrm{dBm/Hz}] - 10\log_{10}(B[\mathrm{Hz}]) + 2G_{\lhd}[\mathrm{dB}] - 69.6$ is a scalar, $\mathbb{E}\{\bullet\}$ is the expectation operator, $\mathrm{erf}[\bullet]$ is the error function [5], and $f_{D_M}(\bullet)$ is the probability density function (PDF) of D_M. Note that, in (8), (a) is due to $\rho \sim N(0, \sigma^2)$.

The data transmission latency $T_{\mathrm{one}}(\bullet)$ incurred over the typical single-hop link is given as

$$T_{\mathrm{one}}\left(\mathrm{SNR}\right) = \frac{P_S}{R} = \frac{P_S}{\left(1 - \frac{\tau}{t_t}\right) B\log_2\left(1 + \mathrm{SNR}\right)}. \quad (10)$$

For multi-hop V2V communications, the overall transmission latency, which depends on both the transmission latency and the processing latency in each hop, is a random variable and a detailed modeling is prohibitive. For a tractable analysis, in this paper, we estimate the average transmission latency in the V2V multi-hop links, referred to as the multi-hop latency hereinafter, by

$$T_{\mathrm{mul}} = \mathbb{E}(K)\mathbb{E}\left(T_{\mathrm{one}}\right) + \left[\mathbb{E}(K) - 1\right] t_{\mathrm{pro}}, \quad (11)$$

where $\mathbb{E}(K)$ is the average hop count required to complete the message transmission from V_t to V_d, and t_{pro} is the latency incurred for processing the mmWave signal at each relay AV. Let Z be the FP of a typical single-hop link, which measures the distance traveled towards its final destination in the considered single hop [6]. According to [37], we can estimate the average hop count of the V2V multi-hop links by

$$\mathbb{E}(K) \approx d_0/\mathbb{E}(Z). \quad (12)$$

Substituting (10) and (12) into (11), the multi-hop latency is given as

$$T_{\mathrm{mul}} = \frac{d_0}{\mathbb{E}(Z)} \int_0^{+\infty} \frac{P_S}{\left(1 - \frac{\tau}{t_t}\right) B\log_2\left(1 + \gamma\right)} dF_{\mathrm{SNR}}\left(\gamma\right) + \left[\frac{d_0}{\mathbb{E}(Z)} - 1\right] t_{\mathrm{pro}}. \quad (13)$$

2) Reliability Analysis: The transmission reliability of the typical single-hop link is defined as

$$P_{\mathrm{one}} = \mathbb{P}\left(\mathrm{SNR} \geqslant \varepsilon\right) = 1 - F_{\mathrm{SNR}}\left(\varepsilon\right), \quad (14)$$

which characterizes the likelihood that the SNR of the typical single-hop link exceeds a given threshold ε required for reliable packet decoding/reception at the receiving AVs [38]. Moreover, the transmission reliability of the multi-hop V2V links, referred to as the multi-hop reliability hereinafter, is given as

$$P_{\mathrm{mul}} = P_{\mathrm{one}}^{\mathbb{E}(K)} = \left[1 - F_{\mathrm{SNR}}\left(\varepsilon\right)\right]^{\mathbb{E}(K)}. \quad (15)$$

We note that both the CDF of SNR, $F_{\mathrm{SNR}}(\varepsilon)$, and the average single-hop latency, $\mathbb{E}(T_{\mathrm{one}})$, decrease with the average hop count, $\mathbb{E}(K)$, which depends on the adopted relay selection scheme. Therefore, the overall impact of $F_{\mathrm{SNR}}(\varepsilon)$ and $\mathbb{E}(T_{\mathrm{one}})$ on T_{mul} and P_{mul} has to be evaluated specifically for different relay selection schemes.

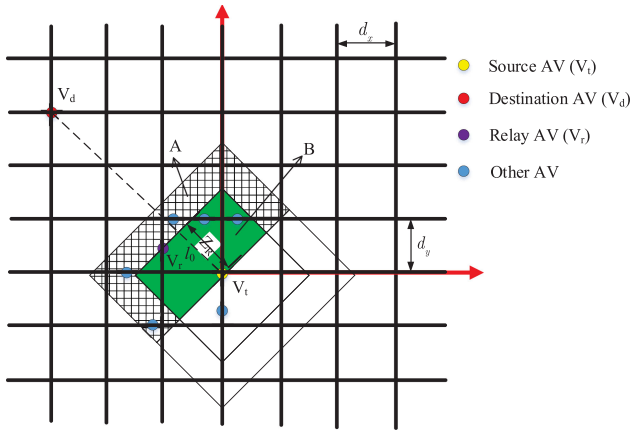

Fig. 3. Single-hop FP under RFP relay selection scheme.

III. Performance Analysis of Existing V2V Relay Selection Schemes With SED Headway

Based on the SED headway and the mmWave propagation models, in this section, we analyze the performance of several existing relay selection schemes in the mmWave multi-hop V2V network. We consider the well-known MFR, NFP and RFP schemes [6], [39], whereby the AV with the largest FP, the AV with the smallest FP, and a random AV within the effective communication range is chosen as the relay AV, respectively. These relay selection schemes generate different FPs in each hop, which further impact the required hop count, latency and reliability of mmWave multi-hop V2V communications. The performance of these schemes is evaluated to uncover the intricate couplings between latency, reliability and FP. Furthermore, the performance analysis provides a basis for intelligent relay selection design in Section IV.

Lemma 1: Let $d(\mathrm{E})$ and $S(\mathrm{E})$ be the road length and the area covered by a taxicab circle E, we have $d(\mathrm{E}) \approx \eta S(\mathrm{E})$, where $\eta = \frac{1}{d_x} + \frac{1}{d_y}$.

Proof: Please refer to Appendix A. ■

We note that Lemma 1 is consistent with the measurement result in [40], where the road length covered by an arbitrary region in a large geography is also shown to be proportional to the area of the region. Lemma 1 provides the basis for performance analysis throughout this section.

A Cartesian coordinate system as shown in Fig. 3 is created for the purpose of analysis, where the origin $(0, 0)$ coincides with AV V_t. Without loss of generality, we assume that AV V_d is located at $(-\frac{d_0}{\sqrt{2}}, \frac{d_0}{\sqrt{2}})$. Line segment V_tV_d and the horizontal axis form an angle of 135°.

A. RFP Relay Selection Scheme

We first consider the RFP relay selection scheme, which is the simplest among the considered schemes. The single-hop FP under RFP relay selection scheme is given by Z_R, i.e., the projection of line segment V_rV_t along V_dV_t for relay AV located at V_r, cf. Fig. 3. Let A and B denote the shaded and the colored (green) regions, respectively. By employing the RFP

scheme [39], an AV within region A ∪ B is randomly selected for message forwarding provided $Z_R > 0$.

1) Average Hop Count Under RFP Relay Selection Scheme: Let l_0 be the intersection of line segment V_tV_d and region A ∪ B, which also results in a line segment. Since the relay AV is randomly selected within region A ∪ B, Z_R is uniformly distributed in l_0 under RFP. Therefore, the CDF of the single-hop FP under RFP can be obtained as $F_{Z_R}(z_R) = \frac{\sqrt{2}z_R}{d_t}$, where $0 \leqslant z_R \leqslant \frac{d_t}{\sqrt{2}}$. Correspondingly, the probability density function (PDF) of the single-hop FP under RFP is

$$f_{Z_R}(z_R) = \frac{dF_{Z_R}(z_R)}{dz_R} = \frac{\sqrt{2}}{d_t}, 0 \leqslant z_R \leqslant \frac{d_t}{\sqrt{2}}. \quad (16)$$

Substituting (20) into (12), the hop count under RFP is derived as

$$\mathbb{E}(K_R) = \frac{d_0}{\mathbb{E}(Z_R)} = \frac{d_0}{\int_0^{\frac{d_t}{\sqrt{2}}} z_R f_{Z_R}(z_R)\, dz_R} = \frac{2\sqrt{2}d_0}{d_t}. \quad (17)$$

2) Multi-Hop Latency and Reliability Under RFP Relay Selection Scheme:

Lemma 2: the PDF of the Manhattan distance between V_t and the selected relay AV under RFP is given by

$$f_{D_{M_R}}(d_{M_R}) = \frac{2d_{M_R}}{d_t^2}, 0 \leqslant d_{M_R} \leqslant d_t. \quad (18)$$

Proof: Please refer to Appendix B. ■

Substituting (18) into (8), the CDF of SNR in the single-hop link under RFP is obtained as

$$F_{\mathrm{SNR}_R}(\gamma_R) = \frac{1}{2} - \frac{1}{2}\int_0^{d_t} W(\gamma_R, d_{M_R}) \frac{2d_{M_R}}{d_t^2} dd_{M_R}. \quad (19)$$

Finally, substituting (17) and (19) into (13), the multi-hop latency under RFP can be derived as $T_{\mathrm{mul}_R} = \frac{2\sqrt{2}d_0}{d_t}\int_0^{+\infty} T_{\mathrm{one}}(\gamma_R) dF_{\mathrm{SNR}_R}(\gamma_R) + (\frac{2\sqrt{2}d_0}{d_t} - 1)t_{\mathrm{pro}}$.

Based on (17) and (19), the multi-hop reliability under RFP is derived as

$$P_{\mathrm{mul}_R} = [1 - F_{\mathrm{SNR}_R}(\varepsilon)]^{\mathbb{E}(K_R)} = \left[\frac{1}{2} + \frac{1}{2}\int_0^{d_t} W(\varepsilon, d_{M_R}) \frac{2d_{M_R}}{d_t^2} dd_{M_R}\right]^{\frac{2\sqrt{2}d_0}{d_t}}. \quad (20)$$

B. MFR and NFP Relay Selection Schemes

Next, we consider the MFR and NFP relay selection schemes. As illustrated in Fig. 4, Z_x denotes the single-hop FP under relay selection scheme x, where subscript $x \in \{F, N\}$ refers to the MFR and NFP schemes, respectively. Moreover, denote the shaded and the colored (yellow) regions by C and D, respectively. For the MFR (NFP) scheme, the AV generating the largest (smallest) FP among all AVs within the effective communication range of V_t, which is located in the second quadrant, i.e., within region C ∪ D, and can be reached from V_t via a single-hop communication link, will be selected for message forwarding.

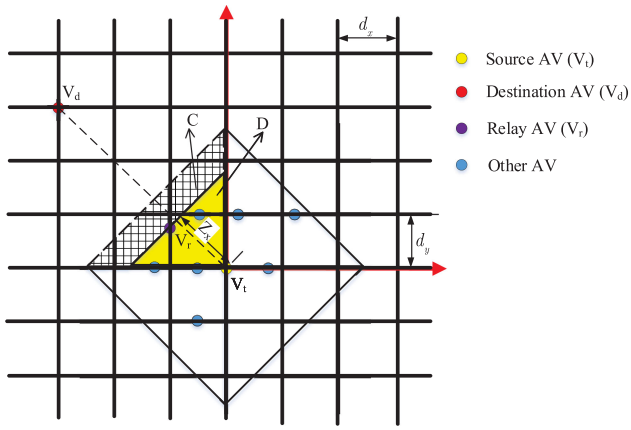

Fig. 4. Single-hop FP under MFR and NFP relay selection schemes.

We note that, the MFR (NFP) scheme in [6] and [39] only constrains the candidate relay AVs to be within the effective communication range of V_t and having positive FP, rather than within C ∪ D. However, this may cause a large number of hops before or even without reaching the destined AV V_d. Different from [6] and [39], this problem is avoided herein.

1) Average Hop Count Under MFR Relay Selection Scheme:

Lemma 3: If $0 \leqslant d_s \leqslant \frac{1}{4}\eta d_t^2$, the PDF of the single-hop FP under MFR is given as

$$f_{Z_F}(z_F) = \begin{cases} \frac{2\mu\eta z_F e^{\mu\left(d_s+\eta z_F^2\right)}}{e^{\frac{\mu\eta d_t^2}{2}} - e^{d_s\mu}}, & \text{for } \sqrt{\frac{d_s}{\eta}} < z_F \leqslant \sqrt{\frac{1}{2}d_t^2 - \frac{d_s}{\eta}}, \\ \frac{2\mu\eta z_F e^{-\mu\left(\eta z_F^2 - d_s\right)}}{1 - e^{-\mu\left(\frac{\eta d_t^2}{2} - d_s\right)}}, & \text{for } \sqrt{\frac{1}{2}d_t^2 - \frac{d_s}{\eta}} < z_F \leqslant \frac{d_t}{\sqrt{2}}. \end{cases} \quad (21)$$

Moreover, if $\frac{1}{4}\eta d_t^2 \leqslant d_s < \frac{1}{2}\eta d_t^2$, we have

$$f_{Z_F}(z_F) = \frac{2\mu\eta z_F e^{-\mu\left(\eta z_F^2 - d_s\right)}}{1 - e^{-\mu\left(\frac{\eta d_t^2}{2} - d_s\right)}}, \text{ for } \sqrt{\frac{d_s}{\eta}} < z_F \leqslant \frac{d_t}{\sqrt{2}}. \quad (22)$$

Proof: Please refer to Appendix C. ■

When $0 \leqslant d_s \leqslant \frac{1}{4}\eta d_t^2$, the average hop count required by MFR is derived by substituting (21) and (22) into (12),

$$\mathbb{E}(K_F) = \frac{d_0}{\mathbb{E}(Z_F)} = \frac{d_0}{\left[\int_{\sqrt{\frac{d_s}{\eta}}}^{\sqrt{\frac{1}{2}d_t^2 - \frac{d_s}{\eta}}} z_F \frac{2\mu\eta z_F e^{\mu\left(d_s+\eta z_F^2\right)}}{e^{\frac{\mu\eta d_t^2}{2}} - e^{d_s\mu}} dz_F + \int_{\sqrt{\frac{1}{2}d_t^2 - \frac{d_s}{\eta}}}^{\frac{d_t}{\sqrt{2}}} z_F \frac{2\mu\eta z_F e^{-\mu\left(\eta z_F^2 - d_s\right)}}{1 - e^{-\mu\left(\frac{\eta d_t^2}{2} - d_s\right)}} dz_F\right]}. \quad (23)$$

Similarly, when $\frac{1}{4}\eta d_t^2 \leqslant d_s < \frac{1}{2}\eta d_t^2$, we have

$$\mathbb{E}(K_F) = \frac{d_0}{\mathbb{E}(Z_F)} = \frac{d_0}{\int_{\sqrt{\frac{d_s}{\eta}}}^{\frac{d_t}{\sqrt{2}}} z_F \frac{2\mu\eta z_F e^{-\mu\left(\eta z_F^2 - d_s\right)}}{1-e^{-\mu\left(\frac{\eta d_t^2}{2}-d_s\right)}} dz_F}. \quad (24)$$

2) Multi-Hop Latency and Reliability Under MFR Relay Selection Scheme: According to Fig. 4, the Manhattan distance between the source AV and the relaying AV under MFR is $D_{M_F} = \sqrt{2}Z_F$. Based on Lemma 3, the PDF of the Manhattan distance between the source AV and the relay AV under MFR is given as

$$f_{D_{M_F}}(d_{M_F}) = \frac{1}{\sqrt{2}} f_{Z_F}\left(\frac{d_{M_F}}{\sqrt{2}}\right). \quad (25)$$

Consequently, if $0 \leqslant d_s \leqslant \frac{1}{4}\eta d_t^2$, the CDF of SNR in the single-hop link under MFR is given as

$$F_{\text{SNR}_F}(\gamma_F) = \frac{1}{2} - \frac{1}{2} \times \left\{ \int_{\sqrt{\frac{2d_s}{\eta}}}^{\sqrt{d_t^2 - \frac{2d_s}{\eta}}} W(\gamma_F, d_{M_F}) \frac{\mu\eta d_{M_F} e^{\mu\left(d_s + \eta d_{M_F}^2/2\right)}}{e^{\mu\eta d_t^2/2} - e^{d_s\mu}} dd_{M_F} + \int_{\sqrt{d_t^2 - \frac{2d_s}{\eta}}}^{d_t} W(\gamma_F, d_{M_F}) \frac{\mu\eta d_{M_F} e^{\mu\left(d_s - \eta d_{M_F}^2/2\right)}}{1 - e^{\mu\left(d_s - \eta d_t^2/2\right)}} dd_{M_F} \right\}. \quad (26)$$

On the other hand, if $\frac{1}{4}\eta d_t^2 \leqslant d_s < \frac{1}{2}\eta d_t^2$, we have

$$F_{\text{SNR}_F}(\gamma_F) = \frac{1}{2} - \frac{1}{2} \times \int_{\sqrt{\frac{2d_s}{\eta}}}^{d_t} W(\gamma_F, d_{M_F}) \frac{\mu\eta d_{M_F} e^{-\mu\left(\eta d_{M_F}^2/2 - d_s\right)}}{1 - e^{-\mu\left(\eta d_t^2/2 - d_s\right)}} dd_{M_F}. \quad (27)$$

Finally, substituting (25)–(27) into (13), the multi-hop latency under MFR is derived as $T_{\text{mul}_F} = \mathbb{E}(K_F)\int_0^{+\infty} T_{\text{one}}(\gamma_F) dF_{\text{SNR}_F}(\gamma_F) + [\mathbb{E}(K_F) - 1]t_{\text{pro}}$.

Based on (23)–(27), the multi-hop reliability under MFR is derived as

$$P_{\text{mul}_F} = \left[1 - F_{\text{SNR}_F}(\varepsilon)\right]^{\mathbb{E}(K_F)}. \quad (28)$$

3) Average Hop Count Under NFP Relay Selection Scheme:

Lemma 4: The PDF of the single-hop FP under NFP is given by

$$f_{Z_N}(z_N) = \frac{2\mu\eta z_N e^{-\mu\left(\eta z_N^2 - d_s\right)}}{1-e^{-\mu\left(\eta d_t^2/2 - d_s\right)}}, \text{ for } \sqrt{\frac{d_s}{\eta}} \leqslant z_N \leqslant \frac{d_t}{\sqrt{2}}. \quad (29)$$

Proof: Please refer to Appendix D. ■

Substituting (29) into (12), the average hop count under NFP is derived as

$$\mathbb{E}(K_N) = \frac{d_0}{\mathbb{E}(Z_N)} = \frac{d_0}{\int_{\sqrt{\frac{d_s}{\eta}}}^{\frac{d_t}{\sqrt{2}}} z_N \frac{2\mu\eta z_N e^{-\mu\left(\eta z_N^2 - d_s\right)}}{1-e^{-\mu\left(\eta d_t^2/2 - d_s\right)}} dz_N}. \quad (30)$$

4) Multi-Hop Latency and Reliability Under NFP Relay Selection Scheme: Similar to MFR, the Manhattan distance between the source AV and the relay AV under NFP satisfies $D_{M_N} = \sqrt{2}Z_N$. Following the same approach as in Section III-B-(2), the multi-hop latency under NFP can be expressed as $T_{\text{mul}_N} = \mathbb{E}(K_N)\int_0^{+\infty} T_{\text{one}}(\gamma_N) dF_{\text{SNR}_N}(\gamma_N) + [\mathbb{E}(K_N) - 1]t_{\text{pro}}$, where the CDF of SNR in the single-hop link under NFP is given as

$$F_{\text{SNR}_N}(\gamma_N) = \frac{1}{2} - \frac{1}{2} \times \int_{\sqrt{\frac{2d_s}{\eta}}}^{d_t} W(\gamma_N, d_{M_N}) \frac{\mu\eta d_{M_N} e^{-\mu\left(\eta d_{M_N}^2/2 - d_s\right)}}{1 - e^{-\mu\left(\eta d_t^2/2 - d_s\right)}} dd_{M_N}. \quad (31)$$

Based on (30) and (31), the multi-hop reliability under NFP is derived as

$$P_{\text{mul}_N} = \left[1 - F_{\text{SNR}_N}(\varepsilon)\right]^{\mathbb{E}(K_N)}. \quad (32)$$

IV. Proposed V2V Relay Selection Scheme and Performance Analysis

The relay selection schemes investigated in Section III only consider the single-hop FP for low computational complexity, while the impact on multi-hop latency is ignored. Consequently, these relay selection schemes may suffer from high multi-hop latency. To mitigate this problem, in this section, a novel V2V relay selection scheme based on joint optimization of single-hop FP and latency is proposed for low-latency message transmission in V2V multi-hop links while guaranteeing the multi-hop reliability.

A. Optimization Problem Formulation

As the statistical modeling of AVs' locations in Section II may not facilitate accurate decisions for message forwarding at an individual AV [41], throughout this section, we consider AVs' instantaneous locations for the algorithm design. In particular, let Φ_i denote the set of AVs located within the effective communication range of a host AV, V_i, and having positive FP towards the destination AV. We assume that AV V_i knows only the locations of the AVs in Φ_i and the destination AV, other than the locations of remote AVs existing beyond its transmission range. Based on this location information, AV V_i selects the next relay AV from set Φ_i to continue the message forwarding. As such, each relay AV forwards the messages on a best-effort basis until reaching the destination AV. The optimization problem aims to minimize the multi-hop latency while ensuring the SNR of each single-hop link averaged over shadowing to be at least ε_0, which can be formulated as

$$\min_{V_{i+1} \in \Phi_i} \quad T_{\text{mul}} \quad \text{s.t.} \quad \mathbb{E}(\text{SNR}) \geqslant \varepsilon_0, \quad (33)$$

where the expectation $\mathbb{E}\{\bullet\}$ is taken over shadowing. Since the transmission reliability of each single-hop link is defined as the likelihood that the SNR of each single-hop link exceeds a given threshold ε, the constraint in (33) guarantees reliable multi-hop transmission on average when $\varepsilon_0 \geqslant \varepsilon$.

Algorithm 1: Proposed Relay Selection Scheme.

Begin:

1: Initialize the locations of all AVs and SNR threshold ε_0, set $\Phi_p = \emptyset$, identify the source AV V_t and the destination AV V_d, and set $Q = Q_{\max}$, $T_{\mathrm{mul}_O} = 0$ and $V_r = V_t$;
2: **while** $(V_r \neq V_d)$&&$(V_d$ is not within the effective communication range of $V_r)$ **do**
3: Calculate the Euclidean distance D_i between V_r and V_d;
4: Get the set $\Phi_r' = \{V_1, V_2, \ldots, V_{|\Phi_r'|}\}$ of all AVs satisfying $\mathbb{E}(\mathrm{SNR}) \geqslant \varepsilon_0$ and $FP > 0$ within the effective communication range of V_r;
5: **for** j = 1:1: $|\Phi_r'|$ **do**
6: Calculate the single-hop FP and single-hop latency generated by message transmission from V_r to V_j;
7: **if** $\frac{D_i}{Z_j} \times T_j + (\frac{D_i}{Z_j} - 1) \times t_{\mathrm{pro}} \leqslant Q$ **then**
8: $Q = \frac{D_i}{Z_j} \times T_j + (\frac{D_i}{Z_j} - 1) \times t_{\mathrm{pro}}$, $V_{\mathrm{temp}} = V_j$, $T_{\mathrm{temp}} = T_j$;
9: $T_{\mathrm{mul}_O} = T_{\mathrm{mul}_O} + T_{\mathrm{temp}}$, $V_r = V_{\mathrm{temp}}$;
10: **if** $V_r \neq V_d$ **then**
11: Add V_r to set Φ_p;
12: $T_{\mathrm{mul}_O} = T_{\mathrm{mul}_O} + t_{\mathrm{pro}}$;
13: Calculate the message transmission latency T_{last} from V_r to V_d;
14: $T_{\mathrm{mul}_O} = T_{\mathrm{mul}_O} + T_{\mathrm{last}}$;
15: Φ_p is the set of selected relay AVs under PRS, and the multi-hop latency is T_{mul_O}.

This problem is non-convex due to the non-convex objective and constraint functions as well as the discrete set Φ_i, which is generally NP-hard. To strike a balance between performance and computational complexity, in the following, we propose a suboptimal scheme to solve this problem.

B. Proposed Relay Selection Scheme

As shown in Fig. 5, given the current transmitter V_i, the proposed relay selection (PRS) scheme selects the relaying AV V_{i+1} that minimizes the multi-hop latency according to the following selection criterion

$$V_{i+1} = \arg\min_{V_j \in \Phi_i'} \left[\frac{D_i}{Z_j} \times T_j + \left(\frac{D_i}{Z_j} - 1 \right) \times t_{\mathrm{pro}} \right]. \quad (34)$$

Herein, motivated by the performance analysis in Section III, the objective function is defined as the residual multi-hop latency required for completing the message transmission to destined AV V_d. $\Phi_i' \subseteq \Phi_i$ is a set of AVs that satisfy the constraint $\mathbb{E}(\mathrm{SNR}) \geqslant \varepsilon_0$. D_i is the distance between the current transmitter V_i and the destination AV V_d. Finally, Z_j and T_j are the single-hop FP and the single-hop latency when V_j is selected as the relay AV, respectively, whereby $\frac{D_i}{Z_j}$ gives the average residual hop count. Algorithm 1 depicts the PRS scheme in detail. We note that the proposed relay selection scheme takes into account both the instantaneous location information of AVs in Φ_i' and the potential latency over residual hops for minimization of the multi-hop latency.

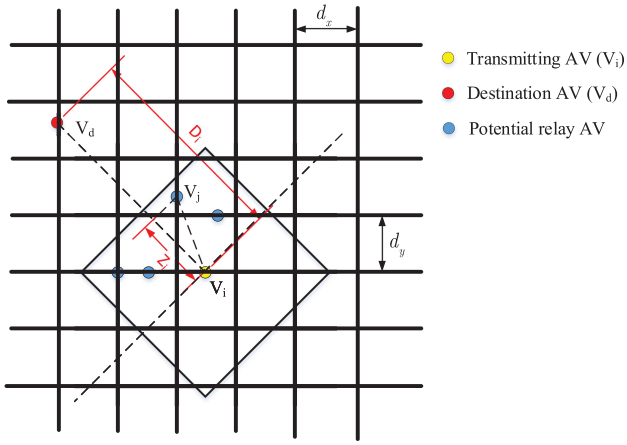

Fig. 5. Proposed V2V relay selection scheme based on joint optimization of single-hop FP and latency.

C. Multi-Hop Latency Analysis

Theorem 1: With the PRS scheme, the minimum multi-hop latency required for message transmission from V_t to V_d is given by

$$T_{\mathrm{mul}_O} = \int_0^{+\infty} \zeta dF_{T_{\mathrm{mul}_O}}(\zeta), \quad (35)$$

with $F_{T_{\mathrm{mul}_O}}(\zeta)$ given by (36), shown at the bottom of the next page.

Proof: Please refer to Appendix E. ■

V. Simulation Results

In this section, we evaluate the multi-hop latency and reliability performance for the considered V2V relay selection schemes via Monte Carlo simulations. Unless specified, otherwise the simulation parameters are set according to Table II.

Fig. 6(a) and (b) show the multi-hop latency and reliability as functions of the effective communication range of the AVs, d_t, for different V2V relay selection schemes. We observe from Fig. 6(a) and (b) that, for MFR, RFP and PRS with small d_ts, the performance improves by increasing d_t, leading to reduced multi-hop latency and increased multi-hop reliability. This is because, for small communication ranges, the single-hop transmission latency is low while the single-hop transmission reliability is close to one. In this case, for MFR, RFP and PRS, increasing d_t enables AVs with a larger single-hop FP to be selected for message relaying, which reduces the number of hops required for completing the message forwarding and improves both multi-hop latency and reliability. However, when d_t becomes large, the performance of MFR and RFP deteriorates quickly as d_t increases. This is because, despite of a reduced number of required communication hops, the latency and the reliability of each single-hop transmission degrade drastically

TABLE II
SIMULATION PARAMETERS

Parameter	Value	Parameter	Value
Distance between V_t and V_d	$d_0 = 500\sqrt{2}$ m	Transmit power	$P_{\rm tx} = 30$ dBm [42]
Noise spectral density	$N_0 = -174$ dBm/Hz [43]	Bandwidth of mmWave signals	$B = 200$ MHz [5]
Interval of adjacent roads	$d_x = d_y = 50$ m	Transmission duration	$t_t = 4$ ms [44]
Pilot transmission duration	$t_p = 0.2$ ms [11]	Processing latency at relay AV	$t_{\rm pro} = 20$ μs [45]
Sector-level beamwidth	$\psi_{i,j}^{\rm tx} = \psi_{i,j}^{\rm rx} = 40^{\rm o}$ [46]	Beam-level beamwidth	$\varphi_{i,j}^{\rm tx} = \varphi_{i,j}^{\rm rx} = 10^{\rm o}$
Main-lobe antenna gain	$G_{\triangleleft} = 13$ dB [47]	SNR threshold	$\varepsilon = \varepsilon_0 = 5$ dB [17]
Standard deviation of shadowing	$\sigma = 4$ dB [48]	Packet size of message	$P_S = 24000$ bits [50]

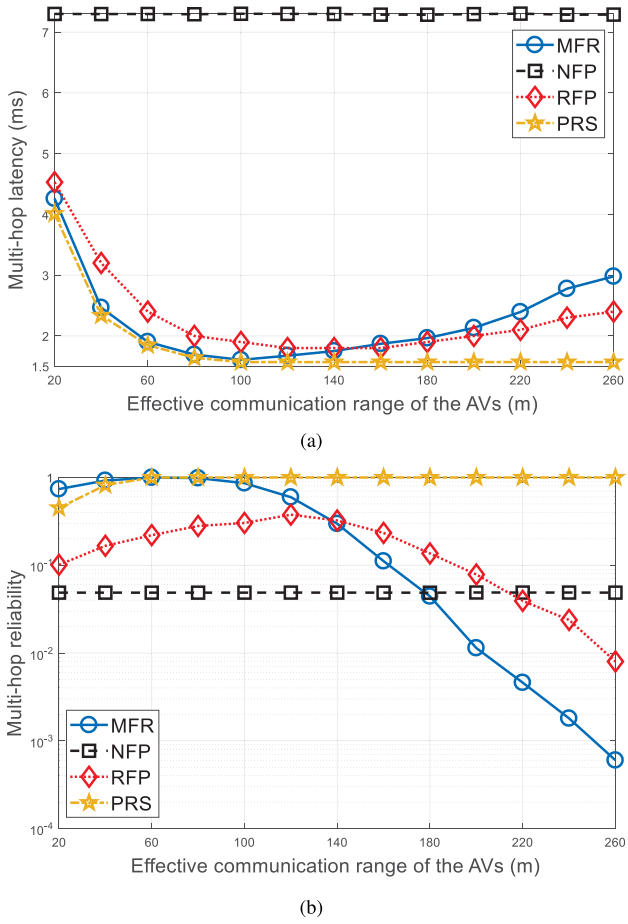

Fig. 6. (a) Multi-hop latency (in linear scale) and (b) multi-hop reliability (in logarithmic scale) versus effective communication range of the AVs for the considered V2V relay selection schemes ($\mu = 0.4$, $\alpha = 3.2$, $d_s = 4$ m).

and compromise the performance of overall multi-hop communications. Similarly, due to the performance bottleneck caused by communication hops of large FPs, MFR is even outperformed by RFP in the large d_t regime. In contrast, for PRS, both the multi-hop latency and reliability *saturate* when d_t becomes large, e.g., when d_t exceeds 100 m for the considered simulation setup. This is because, for the PRS scheme, the relay AV selected in each hop has to guarantee a minimum average signal-to-noise ratio (SNR) such that $\mathbb{E}(\text{SNR}) \geqslant \varepsilon_0$, cf. (33). Given the simulation parameters in Table II, the set of AV candidates satisfying the SNR requirement are always limited to the taxicab circle with radius of 100 meters, whereby increasing d_t cannot further improve the performance of the proposed PRS scheme.

From Fig. 6(a) and (b) we also observe that the multi-hop latency and reliability under NFP rarely change with the effective communication range of the AVs for all considered d_ts. This is because the NFP always selects the AV closest to the current transmitter as the relay AV for message forwarding. Moreover, although the MFR and RFP schemes outperform NFP in both multi-hop latency and reliability when d_t is small, the NFP scheme excels in multi-hop reliability when d_t becomes large. Nevertheless, by jointly exploiting the location information of AVs within the transmission range of each hop and the stochastic geometry based latency analysis for the multi-hop V2V network, the proposed PRS scheme outperforms the MFR, NFP and RFP in both multi-hop latency and reliability, except for small d_ts. In the latter case, the PRS scheme may select communication hops with small FPs for minimization of the multi-hop latency, whereas the increased number of hops slightly lowers its multi-hop reliability.

Fig. 7(a) and (b) evaluate the multi-hop latency and reliability as functions of the path loss exponent for the considered V2V relay selection schemes. From Fig. 7(a) and (b) we observe that

$$F_{T_{\text{mul}_O}}(\zeta) = 1 - \left[1 - \int_{P_S}^{+\infty} \left\{1 - \frac{\sqrt{2}d_0\left[T_{\text{one}}(\gamma_R) + t_{\text{pro}}\right]}{d_t(\zeta + t_{\text{pro}})}\right\} f_{\text{SNR}_R}(\gamma_R)\, d\gamma\right]^{\lambda\eta\left[\min\left(d_t, 10^{\frac{u-\varepsilon_0}{10\alpha}}\right)\right]^2} \Bigg/ 2^{B\left(1-\frac{\tau}{t_t}\right)\left(\frac{d_t(\zeta+t_{\text{pro}})}{\sqrt{2}d_0} - t_{\text{pro}}\right)} - 1 \tag{36}$$

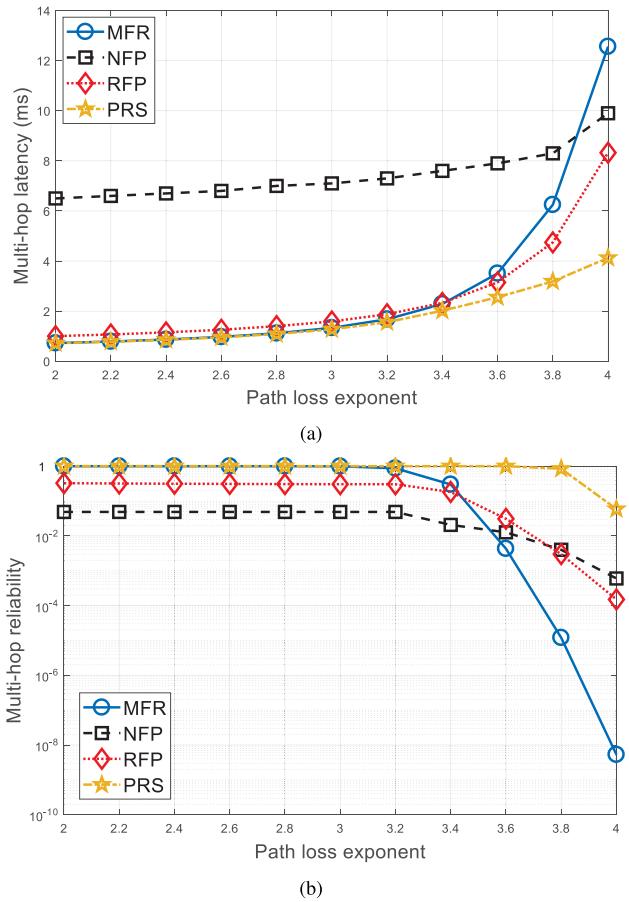

Fig. 7. (a) Multi-hop latency (in linear scale) and (b) multi-hop reliability (in logarithmic scale) versus path loss exponent for the considered V2V relay selection schemes ($\mu = 0.2$, $d_t = 100$ m, $d_s = 4$ m).

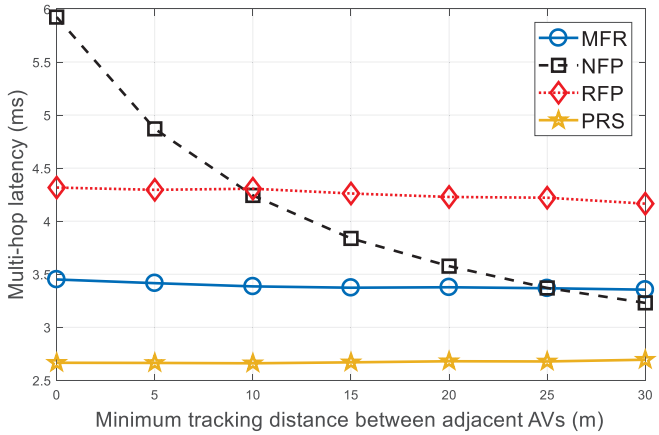

Fig. 8. Multi-hop latency versus minimum tracking distance between adjacent AVs for the considered V2V relay selection schemes ($\mu = 0.08$, $\alpha = 3.3$, $d_t = 100$ m, $G_{\triangleleft} = 10$ dB).

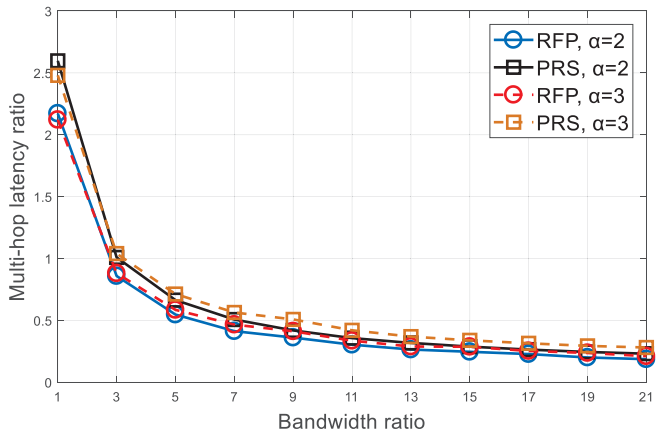

Fig. 9. Multi-hop latency ratio versus the bandwidth ratio for RFP and PRS schemes under different path loss exponents (The bandwidth of the 5.9 GHz signals is fixed as 10 MHz, $G_{\triangleleft} = 10$ dB).

the multi-hop latency increases with the path loss exponent, whereas the multi-hop reliability decreases with the path loss exponent. This is because, as the path loss exponent increases, the path loss of mmWave signals in the single-hop link enlarges. This degrades the SNR of the single-hop link, leading to increased multi-hop latency and reduced multi-hop reliability. From Fig. 7(a) and (b) we also observe that the proposed PRS scheme outperforms the MFR, NFP and RFP in multi-hop latency and reliability for the considered path loss exponent values.

Fig. 8 shows the multi-hop latency as a function of the minimum tracking distance between adjacent AVs for the considered V2V relay selection schemes. From Fig. 8, we observe that, for MFR, RFP and PRS, the multi-hop latency only decreases slowly with the minimum tracking distance between adjacent AVs, d_s. In contrast, the multi-hop latency under NFP decreases significantly as d_s increases. This is because, compared with NFP, the AV selected by MFR, RFP and PRS for message forwarding is usually located farther away from the current transmitting AV. That is, the distance between the selected relay AV and current transmitting AV under MFR, RFP and PRS is usually larger than d_s. Consequently, the number of hops required by MFR, RFP and PRS do not vary much as d_s increases. However, by employing NFP, i.e., by selecting the AV closest to the current transmitting AV for message forwarding, the hop count decreases significantly as d_s increases. This leads to a faster decrease of the multi-hop latency by employing NFP than by MFR, RFP and PRS. This result implies that, for modeling the V2V multi-hop network under NFP, the minimum tracking distance between adjacent AVs is a non-negligible factor.

Finally, Fig. 9 shows the multi-hop latency ratio as a function of the bandwidth ratio for RFP and PRS schemes under different path loss exponents. Herein, we define the multi-hop latency ratio as the ratio of the multi-hop latency incurred by 72 GHz mmWave transmission to that incurred by 5.9 GHz transmission. Likewise, we define the bandwidth ratio as B/B', i.e., the ratio of mmWave signals' bandwidth to 5.9 GHz signals' bandwidth. In Fig. 9, we consider sending rapid bursts of 1400 byte-sized packets in the 5.9 GHz band, where B' is fixed as 10 MHz, and sending rapid bursts of 24 000 bit-sized packets in the 72 GHz band with B varying accordingly. From Fig. 9 we observe that the multi-hop latency ratio decreases monotonically with the bandwidth ratio. This is because the mmWave signals

are allocated a larger bandwidth, which increases the effective data rate achievable on each single-hop link and decreases the multi-hop latency. We also observe that, when the bandwidth ratio is between 1 and 3, the 5.9 GHz transmission has a lower multi-hop latency than the 72 GHz mmWave transmission. However, when the bandwidth ratio exceeds 3, the multi-hop latency of 72 GHz mmWave transmission is already much lower than that of 5.9 GHz transmission. These results imply that, in the small bandwidth ratio regime, the multi-hop latency is mainly determined by the path loss associated with signal propagation. However, in the large bandwidth regime, the impact of propagation path loss on multi-hop latency becomes negligible. In the latter case, the large bandwidth of mmWave signals and the resulting abundant degrees of freedom for V2V communications can significantly increase the effective data rate achievable on each single-hop link and reduce the multi-hop latency.

VI. Conclusion

In this article, the latency and reliability of message transmission for AVs in urban scenarios are investigated assuming mmWave multi-hop V2V communications. The SED has been proposed to model the headway of urban grid roads while ensuring a minimum tracking distance between adjacent AVs. Moreover, Manhattan distance is adopted to accurately characterize the mmWave signal propagation distance for urban roads of grid topology. Based on the SED headway model, the multi-hop latency and reliability of V2V message transmission are analyzed for RFP, MFR and NFP, respectively. To improve the performance of message transmission in mmWave V2V multi-hop links, a novel relay selection scheme based on joint optimization of single-hop FP and latency is further proposed. Simulation results show that, by exploiting the location information of AVs within the transmission range of each hop and the residual latency estimate for the multi-hop V2V network, the proposed relay selection scheme outperforms the RFP, MFR and NFP in both multi-hop transmission latency and reliability. In this paper, we have considered only single packet transmission over interference-free mmWave multi-hop V2V communication links. A comparison of the latency and reliability for interference-free and interfering transmissions of large number of packets may be an interesting topic for future research. In this case, the AVs' mobility may notably affect the system performance, which should be carefully evaluated.

Appendix A
Proof of Lemma 1

Assume that the taxicab circle E has radius d_t and hence, an area $S(\mathrm{E}) = 2d_t^2$. The vertical road length covered by E is derived as

$$\begin{aligned} d_v(\mathrm{E}) &= 2d_t + 4\sum_{n=1}^{\left\lfloor \frac{d_t}{d_x} \right\rfloor} (d_t - nd_x) \\ &= 2d_t + 2\left\lfloor \frac{d_t}{d_x} \right\rfloor \left[2d_t - d_x \left(1 + \left\lfloor \frac{d_t}{d_x} \right\rfloor \right) \right]. \end{aligned} \tag{37}$$

Similarly, the horizontal road length covered by E is given as

$$d_h(\mathrm{E}) = 2d_t + 2\left\lfloor \frac{d_t}{d_y} \right\rfloor \left[2d_t - d_y \left(1 + \left\lfloor \frac{d_t}{d_y} \right\rfloor \right) \right]. \tag{38}$$

Therefore, the total road length covered by E is given as

$$\begin{aligned} d(\mathrm{E}) &= d_v(\mathrm{E}) + d_h(\mathrm{E}) \\ &\overset{(b)}{\approx} \left(\frac{1}{d_x} + \frac{1}{d_y} \right) 2d_t^2 \\ &= \eta S(\mathrm{E}), \end{aligned} \tag{39}$$

where (b) follows from the approximations $\left\lfloor \frac{d_t}{d_x} \right\rfloor \approx \frac{d_t}{d_x}$ and $\left\lfloor \frac{d_t}{d_y} \right\rfloor \approx \frac{d_t}{d_y}$.

Appendix B
Proof of Lemma 2

The proof follows a similar approach as in [39]. In particular, by employing RFP, the CDF of the Manhattan distance between the source AV and the relaying AV is given as

$$\begin{aligned} F_{D_{M_R}}(d_{M_R}) &= \frac{d(\mathrm{B})}{d(\mathrm{A} \cup \mathrm{B})} \\ &= \frac{\eta S(\mathrm{B})}{\eta S(\mathrm{A} \cup \mathrm{B})} \\ &= \frac{S(\mathrm{B})}{S(\mathrm{A} \cup \mathrm{B})} = \frac{d_{M_R}^2}{d_t^2}, \end{aligned} \tag{40}$$

where $0 \leqslant d_{M_R} \leqslant d_t$. Finally, the PDF of the single-hop FP under RFP in (18) is obtained by taking the derivative of $F_{D_{M_R}}(d_{M_R})$ with respect to d_{M_R}.

Appendix C
Proof of Lemma 3

Let V_t+ be the event that at least one AV exists in the effective communication range of AV V_t and having positive FP. Moreover, $\Phi(\mathrm{A})$ denotes the set of AVs located within region A and $|\Phi(\mathrm{A})|$ is the cardinality of set $\Phi(\mathrm{A})$. Then, event V_t+ can take place with a probability given by

$$\begin{aligned} \mathbb{P}(V_t+) &= \mathbb{P}\{|\Phi(\mathrm{C} \cup \mathrm{D})| \geqslant 1\} \\ &= \mathbb{P}\{D_{\mathrm{adj}} \leqslant d(\mathrm{C} \cup \mathrm{D})\} \\ &= F_{D_{\mathrm{adj}}}\{\eta[S(\mathrm{C}) + S(\mathrm{D})]\}. \end{aligned} \tag{41}$$

Moreover, when $\mathbb{P}(V_t+) > 0$, the CDF of the single-hop FP under MFR is given by

$$\begin{aligned} F_{Z_F}(z_F) &= \mathbb{P}\{Z_F \leqslant z_F | V_t+\} \\ &\overset{(c)}{=} \frac{\mathbb{P}\{|\Phi(\mathrm{C})| = 0\}\mathbb{P}\{|\Phi(\mathrm{D})| \geqslant 1\}}{\mathbb{P}\{V_t+\}} \\ &= \frac{\mathbb{P}(D_{\mathrm{adj}} > d(\mathrm{C}))\mathbb{P}(D_{\mathrm{adj}} \leqslant d(\mathrm{D}))}{\mathbb{P}\{V_t+\}} \\ &= \frac{\{1 - F_{D_{\mathrm{adj}}}[\eta S(\mathrm{C})]\} F_{D_{\mathrm{adj}}}[\eta S(\mathrm{D})]}{F_{D_{\mathrm{adj}}}\{\eta[S(\mathrm{C}) + S(\mathrm{D})]\}}, \end{aligned} \tag{42}$$

where (c) is due to the fact that Z_F is the maximum FP within region C $\cup$ D, and hence, there is no vehicle in region C but at least one vehicle in region D.

Note that $S(\mathrm{C})+S(\mathrm{D})=\frac{1}{2}d_t^2$, $S(\mathrm{D})=z_F^2$, and $S(\mathrm{C})=\frac{1}{2}d_t^2-z_F^2$. We have $0\leqslant z_F\leqslant\frac{d_t}{\sqrt{2}}$, since $S(\mathrm{C})\geqslant 0$, and $0\leqslant d_s<\frac{1}{2}\eta d_t^2$, since $D_{\mathrm{adj}}\geqslant d_s$.

If $0\leqslant d_s\leqslant\frac{1}{4}\eta d_t^2$, we have $\sqrt{\frac{d_s}{\eta}}\leqslant\sqrt{\frac{1}{2}d_t^2-\frac{d_s}{\eta}}$ and

$$F_{Z_F}(z_F)=\begin{cases}0, & 0\leqslant z_F\leqslant\sqrt{\frac{d_s}{\eta}},\\ \frac{e^{2d_s\mu}-e^{\mu\left(\eta z_F^2+d_s\right)}}{e^{d_s\mu}-e^{\frac{\mu\eta d_t^2}{2}}}, & \sqrt{\frac{d_s}{\eta}}<z_F\leqslant\sqrt{\frac{d_t^2}{2}-\frac{d_s}{\eta}},\\ \frac{1-e^{\mu\left(d_s-\eta z_F^2\right)}}{1-e^{\mu\left(d_s-\eta d_t^2/2\right)}}, & \sqrt{\frac{d_t^2}{2}-\frac{d_s}{\eta}}<z_F\leqslant\frac{d_t}{\sqrt{2}},\\ 1, & z_F>\frac{d_t}{\sqrt{2}}.\end{cases}\tag{43}$$

If $\frac{1}{4}\eta d_t^2\leqslant d_s<\frac{1}{2}\eta d_t^2$, we have $\sqrt{\frac{1}{2}d_t^2-\frac{d_s}{\eta}}\leqslant\sqrt{\frac{d_s}{\eta}}$ and

$$F_{Z_F}(z_F)=\begin{cases}0, & 0\leqslant z_F\leqslant\sqrt{\frac{d_s}{\eta}},\\ \frac{1-e^{-\mu\left(\eta z_F^2-d_s\right)}}{1-e^{-\mu\left(\eta d_t^2/2-d_s\right)}}, & \sqrt{\frac{d_s}{\eta}}<z_F\leqslant\frac{d_t}{\sqrt{2}},\\ 1, & z_F>\frac{d_t}{\sqrt{2}}.\end{cases}\tag{44}$$

Note that the piecewise nature of $F_{Z_F}(z_F)$ follows that of $F_{D_{\mathrm{adj}}}(d_{\mathrm{adj}})$, when $d_s>0$ is taken into account.

Finally, taking the derivative of $F_{Z_F}(z_F)$ with respect to z_F, the PDF of the single-hop FP under MFR is thus given by (21) and (22).

APPENDIX D
PROOF OF LEMMA 4

The proof follows the same approach as in Appendix C. In particular, by employing the NFP, the probability that at least one AV exists in the effective communication range of AV V_t and having positive FP is also given by (41). Therefore, the CDF of the single-hop FP under NFP is derived as

$$\begin{aligned}F_{Z_N}(z_N)&=\mathbb{P}\{Z_N\leqslant z_N|\,V_t+\}\\&=\frac{1-\mathbb{P}\{Z_N>z_N\text{ and }V_t+\}}{\mathbb{P}\{V_t+\}}\\&=\frac{F_{D_{\mathrm{adj}}}[\eta S(\mathrm{D})]}{F_{D_{\mathrm{adj}}}\{\eta[S(\mathrm{C})+S(\mathrm{D})]\}}\\&=\begin{cases}0, & \text{for } 0\leqslant z_N\leqslant\sqrt{\frac{d_s}{\eta}},\\ \frac{1-e^{-\mu\left(\eta z_N^2-d_s\right)}}{1-e^{-\mu\left(\eta d_t^2/2-d_s\right)}}, & \text{for } \sqrt{\frac{d_s}{\eta}}<z_N\leqslant\frac{d_t}{\sqrt{2}},\\ 1, & \text{for } z_N>\frac{d_t}{\sqrt{2}}.\end{cases}\end{aligned}\tag{45}$$

Finally, the PDF of the single-hop FP under NFP in (29) is obtained by taking the derivative of $F_{Z_N}(z_N)$ with respect to z_N.

APPENDIX E
PROOF OF THEOREM 1

For the PRS scheme, $\mathbb{E}(\mathrm{SNR})\geqslant\varepsilon_0$ must be guaranteed in each hop. Substituting $\mathbb{E}(\mathrm{SNR})\geqslant\varepsilon_0$ into (7), we can obtain that $D_M\leqslant 10^{\frac{u-\varepsilon_0}{10\alpha}}$. Therefore, the relay selection region in each hop is a taxicab circle with the current transmitter as its center and $\min(d_t,10^{\frac{u-\varepsilon_0}{10\alpha}})$ as its radius. The average number of AVs within the relay selection region is $\mathbb{E}(N)=\lambda\eta[\min(d_t,10^{\frac{u-\varepsilon_0}{10\alpha}})]^2$.

Let $T_1,T_2,...,T_N$ be the multi-hop latencies corresponding to the AVs within the relay selection region. $T_1,T_2,...,T_N$ are identically distributed as the multi-hop latency under RFP. Let $T_{opt\_1}\leqslant T_{\mathrm{opt\_}2}\leqslant\cdots\leqslant T_{\mathrm{opt\_}N}$ be the non-decreasing sorting of these latencies, where $T_{\mathrm{mul}_O}=T_{\mathrm{opt\_}1}$ is the multi-hop latency by employing PRS. According to the theory of order statistics [50], the CDF of T_{mul_O} is given as

$$F_{T_{\mathrm{mul}_O}}(\zeta)\approx 1-\left[1-F_{T_{\mathrm{mul}_R}}(\zeta)\right]^{\mathbb{E}(N)},\tag{46}$$

where the CDF of the multi-hop latency under RFP can be derived as

$$\begin{aligned}F_{T_{\mathrm{mul}_R}}(\zeta)&=\mathbb{P}(T_{\mathrm{mul}_R}\leqslant\zeta)\\&=\mathbb{P}\left(\frac{d_0}{Z_R}T_{\mathrm{one}}(\gamma_R)+\left(\frac{d_0}{Z_R}-1\right)t_{\mathrm{pro}}\leqslant\zeta\right)\\&=\iint_{\frac{d_0}{Z_R}T_{\mathrm{one}}(\gamma_R)+\left(\frac{d_0}{Z_R}-1\right)t_{\mathrm{pro}}\leqslant\zeta}f(Z_R,\gamma_R)\,dZ_R d\gamma_R\\&=\int_2^{+\infty}\int_{\frac{d_0}{\zeta+t_{\mathrm{pro}}}[T_{\mathrm{one}}(\gamma_R)+t_{\mathrm{pro}}]}^{\frac{d_t}{\sqrt{2}}}f(Z_R)dZ_R d\gamma_R\\&\quad\times\int_{-1}^{\frac{P_S}{B\left(1-\frac{\tau}{t_t}\right)\left(\frac{d_t(\zeta+t_{\mathrm{pro}})}{\sqrt{2}d_0}-t_{\mathrm{pro}}\right)}}f_{\mathrm{SNR}_R}(\gamma_R)\\&=\int_2^{+\infty}\int_{-1}^{\frac{P_S}{\left(B-\frac{B\tau}{t_t}\right)\left(\frac{d_t(\zeta+t_{\mathrm{pro}})}{\sqrt{2}d_0}-t_{\mathrm{pro}}\right)}}\left\{1-\frac{\sqrt{2}d_0}{d_t(\zeta+t_{\mathrm{pro}})}\right.\\&\quad\left.\times[T_{\mathrm{one}}(\gamma_R)+t_{\mathrm{pro}}]\right\}f_{\mathrm{SNR}_R}(\gamma_R)\,d\gamma_R.\end{aligned}\tag{47}$$

Finally, by substituting (47) into (46), the multi-hop latency under the proposed PRS is given in (35).

REFERENCES

[1] X. Ge, "Ultra-reliable low-latency communications in autonomous vehicular networks," *IEEE Trans. Veh. Technol.*, vol. 68, no. 5, pp. 5005–5016, May 2019.

[2] L. Kong, M. K. Khan, F. Wu, G. Chen, and P. Zeng, "Millimeter-wave wireless communications for IoT-cloud supported autonomous vehicles: Overview, design, and challenges," *IEEE Commun. Mag.*, vol. 55, no. 1, pp. 62–68, Jan. 2017.

[3] X. Ge, Z. Li, and S. Li, "5G software defined vehicular networks," *IEEE Commun. Mag.*, vol. 55, no. 7, pp. 87–93, Jul. 2017.

[4] S. Li *et al.*, "Uplinks analysis and optimization of hybrid vehicular networks," *KSII Trans. Internet Inf. Syst.*, vol. 13, no. 2, pp. 473–493, Feb. 2019.

[5] S. Li *et al.*, "Multi-hop links quality analysis of 5G enabled vehicular networks," in *Proc. 9th Int. Conf. Wireless Commun. Signal Process.*, Nanjing, 2017, pp. 1–6.

[6] M. J. Farooq, H. ElSawy, and M. Alouini, "A stochastic geometry model for multi-hop highway vehicular communication," *IEEE Trans. Wireless Commun.*, vol. 15, no. 3, pp. 2276–2291, Mar. 2016.

[7] X. Li *et al.*, "Multi-hop delay reduction for safety-related message broadcasting in vehicle-to-vehicle communications," *IET Commun.*, vol. 9, no. 3, pp. 404–411, Feb. 2015.

[8] J. P. Jeyaraj and M. Haenggi, "Reliability analysis of V2V communications on orthogonal street systems," in *Proc. IEEE Global Commun. Conf.*, Singapore, 2017, pp. 1–6.

[9] M. Ozpolat, E. Kampert, P. A. Jennings, and M. D. Higgins, "A grid-based coverage analysis of urban mmWave vehicular Ad Hoc networks," *IEEE Commun. Lett.*, vol. 22, no. 8, pp. 1692–1695, Aug. 2018.

[10] V. Petrov, J. Kokkoniemi, D. Moltchanov, J. Lehtomki, M. Juntti, and Y. Koucheryavy, "The impact of interference from the side lanes on mmWave/THz band V2V communication systems with directional antennas," *IEEE Trans. Veh. Technol.*, vol. 67, no. 6, pp. 5028–5041, Jun. 2018.

[11] C. Perfecto, J. Del Ser, and M. Bennis, "Millimeter-wave V2V communications: Distributed association and beam alignment," *IEEE J. Sel. Areas Commun.*, vol. 35, no. 9, pp. 2148–2162, Sep. 2017.

[12] Y. Wu, L. Yan, and X. Fang, "A low-latency content dissemination scheme for mmWave vehicular networks," *IEEE Internet Things J.*, vol. 6, no. 5, pp. 7921–7933, Oct. 2019.

[13] M. F. Feteiha and M. H. Ahmed, "Multihop best-relay selection for vehicular communication over highways traffic," *IEEE Trans. Veh. Technol.*, vol. 67, no. 10, pp. 9845–9855, Oct. 2018.

[14] M. Z. Alam, I. Adhicandra, and A. Jamalipour, "Optimal best path selection algorithm for cluster-based multi-hop MIMO cooperative transmission for vehicular communications," *IEEE Trans. Veh. Technol.*, vol. 68, no. 9, pp. 8314–8321, Sep. 2019.

[15] K. Eshteiwi, G. Kaddoum, K. B. Fredj, E. Soujeri, and F. Gagnon, "Performance analysis of full-duplex vehicle relay-based selection in dense multi-lane highways," *IEEE Access*, vol. 7, pp. 61581–61595, Mar. 2019.

[16] G. Sun, L. Song, H. Yu, V. Chang, X. Du, and M. Guizani, "V2V routing in a VANET based on the autoregressive integrated moving average model," *IEEE Trans. Veh. Technol.*, vol. 68, no. 1, pp. 908–922, Jan. 2019.

[17] Y. Wang, K. Venugopal, A. F. Molisch, and R. W. Heath, "MmWave vehicle-to-infrastructure communication: Analysis of urban microcellular networks," *IEEE Trans. Veh. Technol.*, vol. 67, no. 8, pp. 7086–7100, Aug. 2018.

[18] J. G. Andrews, F. Baccelli, and R. K. Ganti, "A tractable approach to coverage and rate in cellular networks," *IEEE Trans. Commun.*, vol. 59, no. 11, pp. 3122–3134, Nov. 2011.

[19] Z. Tong, H. Lu, M. Haenggi, and C. Poellabauer, "A stochastic geometry approach to the modeling of DSRC for vehicular safety communication," *IEEE Trans. Intell. Transp. Syst.*, vol. 17, no. 5, pp. 1448–1458, May 2016.

[20] T. Kimura, H. Saito, H. Honda, and R. Kawahara, "Modeling urban ITS communication via stochastic geometry approach," in *Proc. IEEE 84th Veh. Technol. Conf. (Fall)*, Montreal, QC, 2016, pp. 1–5.

[21] R. J. Cowan, "Useful headway models," *Transp. Res.*, vol. 9, no. 6, pp. 371–375, Dec. 1975.

[22] E. F. Krause, "Taxicab geometry," *Math. Teacher*, vol. 66, no. 8, pp. 695–706, Dec. 1973.

[23] D. Han, B. Bai, and W. Chen, "Secure V2V communications via relays: Resource allocation and performance analysis," *IEEE Wireless Commun. Lett.*, vol. 6, no. 3, pp. 342–345, Jun. 2017.

[24] A. Goldsmith, *Wireless Communications*. Cambridge, U.K.: Cambridge Univ. Press, 2005.

[25] A. Bazzi, B. M. Masini, A. Zanella, and I. Thibault, "On the performance of IEEE 802.11p and LTE-V2V for the cooperative awareness of connected vehicles," *IEEE Trans. Veh. Technol.*, vol. 66, no. 11, pp. 10419–10432, Nov. 2017.

[26] S. Eichler, "Performance evaluation of the IEEE 802.11p wave communication standard," in *Proc. IEEE 66th Veh. Technol. Conf.*, Baltimore, MD, 2007, pp. 2199–2203.

[27] D. Hu, J. Wu, and P. Fan, "Minimizing end-to-end delays in linear multihop networks," *IEEE Trans. Veh. Technol.*, vol. 65, no. 8, pp. 6487–6496, Aug. 2016.

[28] L. Xiang, D. W. K. Ng, T. Islam, R. Schober, V. W. S. Wong, and J. Wang, "Cross-layer optimization of fast video delivery in cache- and buffer-enabled relaying networks," *IEEE Trans. Veh. Technol.*, vol. 66, no. 12, pp. 11366–11382, Dec. 2017.

[29] J. Wildman, P. H. J. Nardelli, M. Latva-aho, and S. Weber, "On the joint impact of beamwidth and orientation error on throughput in directional wireless poisson networks," *IEEE Trans. Wireless Commun.*, vol. 13, no. 12, pp. 7072–7085, Dec. 2014.

[30] A. Ghosh *et al.*, "Millimeter-wave enhanced local area systems: A high-data-rate approach for future wireless networks," *IEEE J. Sel. Areas Commun.*, vol. 32, no. 6, pp. 1152–1163, Jun. 2014.

[31] Y. Oike, M. Ikeda, and K. Asada, "A high-speed and low-voltage associative co-processor with exact Hamming/Manhattan-distance estimation using word-parallel and hierarchical search architecture," *IEEE J. Solid-State Circuits*, vol. 39, no. 8, pp. 1383–1387, Aug. 2004.

[32] K. Zheng, Q. Zheng, H. Yang, L. Zhao, L. Hou, and P. Chatzimisios, "Reliable and efficient autonomous driving: The need for heterogeneous vehicular networks," *IEEE Commun. Mag.*, vol. 53, no. 12, pp. 72–79, Dec. 2015.

[33] C. Perfecto, J. D. Ser, and M. Bennis, "On the interplay between scheduling interval and beamwidth selection for low-latency and reliable V2V mmWave communications," in *Proc. 20th Conf. Innov. Clouds, Internet Netw.*, Paris, 2017, pp. 1–8.

[34] B. Fan, H. Tian, S. Zhu, and X. Zhu, "Traffic-aware relay vehicle selection in millimeter-wave vehicle-to-vehicle communication," *IEEE Wireless Commun. Lett.*, vol. 8, no. 2, pp. 400–403, Apr. 2019.

[35] D. Hu, J. Wu, and P. Fan, "Maximizing end-to-end throughput of interference-limited multihop networks," *IEEE Trans. Veh. Technol.*, vol. 67, no. 6, pp. 5465–5469, Jun. 2018.

[36] X. Ge, K. Huang, C. Wang, X. Hong, and X. Yang, "Capacity analysis of a multi-cell multi-antenna cooperative cellular network with co-channel interference," *IEEE Trans. Wireless Commun.*, vol. 10, no. 10, pp. 3298–3309, Oct. 2011.

[37] S. De, "On hop count and Euclidean distance in greedy forwarding in wireless ad hoc networks," *IEEE Commun. Lett.*, vol. 9, no. 11, pp. 1000–1002, Nov. 2005.

[38] X. Ge, B. Yang, J. Ye, G. Mao, C. Wang and T. Han, "Spatial spectrum and energy efficiency of random cellular networks," *IEEE Trans. Commun.*, vol. 63, no. 3, pp. 1019–1030, Mar. 2015.

[39] M. J. Farooq, H. ElSawy, Q. Zhu, and M. Alouini, "Optimizing mission critical data dissemination in massive IoT networks," in *Proc. 15th Int. Symp. Model. Optim. Mobile, Ad Hoc, Wireless Netw.*, Paris, France, 2017, pp. 1–6.

[40] H. Fang, C. Ren, L. Lin, F. Xiong, and J. Tian, "A road density partition method for the evaluation of road selection," in *Proc. 23rd Int. Conf. Geoinformatics*, Wuhan, China, 2015, pp. 1–6.

[41] X. Ge, J. Ye, Y. Yang, and Q. Li, "User mobility evaluation for 5G small cell networks based on individual mobility model," *IEEE J. Sel. Areas Commun.*, vol. 34, no. 3, pp. 528–541, Mar. 2016.

[42] L. Xiang, X. Ge, C. X. Wang, F. Y. Li, and F. Reichert, "Energy efficiency evaluation of cellular networks based on spatial distributions of traffic load and power consumption," *IEEE Trans. Wireless Commun.*, vol. 12, no. 3, pp. 961–973, Mar. 2013.

[43] T. Zeng, O. Semiari, W. Saad, and M. Bennis, "Integrated communications and control co-design for wireless vehicular platoon systems," in *Proc. IEEE Int. Conf. Commun.*, Kansas City, MO, 2018, pp. 1–6.

[44] C. Perfecto, J. D. Ser, M. Bennis, and M. N. Bilbao, "Beyond WYSIWYG: Sharing contextual sensing data through mmWave V2V communications," in *Proc. Eur. Conf. Netw. Commun.*, Oulu, 2017, pp. 1–6.

[45] Y. Xiao and L. J. Cimini, "Spectral efficiency of distributed cooperative relaying," in *Proc. 45th Annu. Conf. Inf. Sci. Syst.*, Baltimore, MD, 2011, pp. 1–6.

[46] J. Wang *et al.*, "Beam codebook based beamforming protocol for multi-Gbps millimeter-wave WPAN systems," *IEEE J. Sel. Areas Commun.*, vol. 27, no. 8, pp. 1390–1399, Oct. 2009.

[47] T. Bai and R. W. Heath, "Coverage and rate analysis for millimeter-wave cellular networks," *IEEE Trans. Wireless Commun.*, vol. 14, no. 2, pp. 1100–1114, Feb. 2015.

[48] T. S. Rappaport, G. R. MacCartney, M. K. Samimi, and S. Sun, "Wideband millimeter-wave propagation measurements and channel models for future wireless communication system design," *IEEE Trans. Commun.*, vol. 63, no. 9, pp. 3029–3056, Sep. 2015.

[49] "Study on Enhancement of 3GPP Support for 5G V2X Services," 3GPP Tech. Rep. 22.886, Sophia Antipolis Cedex, France, v16.2.0, Dec. 2018.

[50] I. Pitas and A. N. Venetsanopoulos, "Order statistics in digital image processing," *Proc. IEEE*, vol. 80, no. 12, pp. 1893–1921, Dec. 1992.

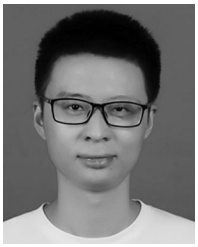

Zipeng Li (Student Member, IEEE) received the B.E. degree in telecommunication engineering and M.S. degree in communication and information system from the Huazhong University of Science and Technology (HUST), Wuhan, China, in 2011 and 2014, respectively. He is currently working toward the Ph.D. degree in HUST. His research interests include vehicular networks, wireless communication networks and autonomous vehicles.

Lin Xiang (Member, IEEE) received the bachelors, and the master's degrees from the Huazhong University of Science and Technology (HUST), China, in 2009 and 2012, respectively, and the Ph.D. degree from the Friedrich-Alexander University of Erlangen-Nuremberg (FAU), Germany, in 2018. He was a Researcher at the University of Luxembourg, Luxembourg, and a Visiting Researcher at the University of Bologna, Italy, and the University of Ljubljana, Slovenia. He is currently a Visiting Research Fellow at the Institute for Digital Communications (IDC), FAU. His research interests include protocol design, performance analysis and optimization of wireless communications, with applications to wireless caching, autonomous drones and vehicles, and smart grid communications. Dr. Xiang was a recipient of the Best Paper Award for IEEE Globecom 2010 and the Erasmus Mundus CONNEC Scholarship. He was an Exemplary Reviewer of the IEEE TRANSACTIONS ON WIRELESS COMMUNICATIONS in 2018 and the IEEE TRANSACTIONS ON COMMUNICATIONS in 2017 and 2018.

Xiaohu Ge (Senior Member, IEEE) received the Ph.D. degree in communication and information engineering from the Huazhong University of Science and Technology (HUST), China, in 2003. He has been working with HUST, since November 2005. Prior to that, he worked as a Researcher at Ajou University, South Korea, and the Politecnico Di Torino, Italy, from January 2004 to October 2005. He is currently a Full Professor with the School of Electronic Information and Communications, HUST. He is also an Adjunct Professor with the Faculty of Engineering and Information Technology, University of Technology Sydney (UTS), Australia. He has published about 200 articles in refereed journals and conference proceedings. He has been granted about 25 patents in China. His research interests are in the area of mobile communications, traffic modeling in wireless networks, green communications, and interference modeling in wireless communications. He services as an IEEE Distinguished Lecturer and an Associate Editor for the IEEE ACCESS, the IEEE WIRELESS COMMUNICATIONS AND THE IEEE TRANSACTIONS ON VEHICULAR TECHNOLOGY, etc.

Guoqiang Mao (Fellow, IEEE) has published over 200 papers in international conferences and journals, which have been cited more than 9000 times. He is an editor of the IEEE TRANSACTIONS ON INTELLIGENT TRANSPORTATION SYSTEMS (since 2018), IEEE TRANSACTIONS ON WIRELESS COMMUNICATIONS (2014–2019), IEEE TRANSACTIONS ON VEHICULAR TECHNOLOGY (since 2010) and received Top Editor Award for outstanding contributions to the IEEE TRANSACTIONS ON VEHICULAR TECHNOLOGY in 2011, 2014 and 2015. He was a Co-Chair of IEEE Intelligent Transport Systems Society Technical Committee on Communication Networks. He has served as a Chair, Co-Chair and TPC Member in a number of international conferences. He is a Fellow of IET. His research interest includes intelligent transport systems, applied graph theory and its applications in telecommunications, Internet of Things, wireless sensor networks, wireless localization techniques and network modeling and performance analysis.

Han-Chieh Chao (Senior Member, IEEE) received the M.S. and Ph.D. degrees in electrical engineering from Purdue University, in 1989 and 1993, respectively. He is a Joint Appointed Full Professor of the Department Computer Science & Information Engineering of National Ilan University (NIU) I-Lan, and Department of Electrical Engineering, National Dong Hwa University (NDHU), Hualien, Taiwan. He was the President during August 2010 to January 2016 for NIU and now is the President of NDHU since February 2016. He was the Director of the Computer Center for Ministry of Education Taiwan from September 2008 to July 2010. His research interests include High Speed Networks, Wireless Networks, IPv6 based Networks, Digital Creative Arts, e-Government, Digital Divide and 5 & 6G Mobile Networks. Dr. Chao has authored or coauthored 4 books and has published about 400 refereed professional research papers. He has completed more than 150 MSEE thesis students and 5 Ph.D. students. Dr. Chao has been invited frequently to give talks at national and international conferences and research organizations. Dr. Chao is the Editor-in-Chief for *Journal of Internet Technology*. Founding Editor-in-Chief for *International Journal of Internet Protocol Technology* and *International Journal of Ad Hoc & Ubiquitous Computing*. Dr. Chao has served as the Associate Editor for *IEEE Wireless Communications, IEEE Network, IEEE Systems Journal and Wireless Communications & Mobile Computing*. Dr. Chao is Fellow of IET (IEE).